Computer simulation of axial channeling in monatomic and diatomic crystals. Multistring model and its application to foreign-atom location

A. Bontemps and J. Fontenille
Centre d'Etudes Nucléaires de Grenoble, Département de Recherche Fondamentale, Section de Physique du Solide, 85 X-38041 Grenoble Cedex, France
(Received 4 January 1978)

A multistring potential with the continuum approximation is used to simulate channeling of charged particles in monatomic and diatomic lattices. Different quantities are calculated: the trajectories, the flux distribution of channeled particles, the close-encounter probability, and angular distribution. The close-encounter yield for foreign atoms present in the channel is also computed and application is made to the lattice location of these atoms in the lattice. Results are given for various crystal types and in particular for bcc, fcc, diamond, and zinc-blende structures. Comparison is made with other computer simulations and, when possible, with experimental results. It is shown that the gross features are in agreement. The discrepancies are discussed.

I. INTRODUCTION

Many theoretical studies of channeling exhibit two dominant features: an investigation of the phenomenon itself and generally its application to the lattice location of foreign atoms in a single crystal. These are the two aims of the computer simulation described in this paper. The investigation of the channeling phenomenon has already been carried out in many cases.[1] Nevertheless, there are relatively few publications on diatomic crystals.[2-6] Our program has thus been designed to study channeling in monatomic as well as diatomic lattices, and to give the interaction yield of channeled particles with interstitial or substitutional foreign atoms.

The different types of computer simulations can be classified with respect to the interaction between the particles and the lattice. Following this classification, the principal models are presented in Table I from the simplest (single-string analytical model) to the most sophisticated (many-body model), together with typical information displayed by the programs. We are concerned essentially with two results which can be compared to experimental channeling data. First, the close-encounter probability with the lattice atoms $\chi(\psi_e, z)$ as a function of ψ_e, the angle between a crystallographic axis and the direction of incident particles and the penetration depth z. This quantity is to be compared to the yield as a function of energy (spectra). Second, the spatial density $n(r,z)$ of the channeled particles which is of fundamental interest in the interpretation of the lattice-location experiments. It can be seen that the multistring model is the simplest one which allows one to obtain both the close-encounter probability and the particle flux as functions of the penetration depth. It must be remarked that, contrary to binary-collision or many-body models, the introduction of thermal vibrations is not adapted to the computational procedure. This problem is discussed in Sec. III. The principles of the computational procedure have been already described in a preliminary communication[8] and more recently such a model has been used to simulate the axial to planar transition.[9] There is some evidence for the use of a similar simulation by Hashimoto[10-12] but to our knowledge no detailed description of this program has been published.

II. COMPUTER MODEL

A. Classical mechanics and continuum approximation

Different criteria define the applicability of classical mechanics to the motion of channeled particles. Comparing quantum-mechanical diffraction and channeling, the classical treatment is found valid if the angular width of the Bragg resonance $\Delta\theta_B$ is much larger than the Bragg angle θ_B.[13] This condition can be written[14]

$$\alpha = \Delta\theta_B/\theta_B = 4mZ_1Z_2e^2/\pi\hbar^2Nd^2 \gg 1\,,$$

where Z_1 and Z_2 are, respectively, the atomic numbers of the incident particle and the target atom, N is the atomic density, and d the interatomic distance along a crystallographic axis. In our case (protons or α's on Si, GaP, ZnTe), the parameter α is of the order of 10^3–10^4. Therefore, classical mechanics will be used for all calculations described here. A second type of criterion proposed by Lindhard[15] concerns the assumption that the continuum approximation is valid. As a basic hypothesis for our model this approximation is done and it is assumed that an atomic row produces at a distance r an average

TABLE I. Comparison of analytical and computer models of channeling.

Model	Analytical	Multistring I	Multistring II	Binary collision	Many-body
Hypotheses	Interaction particle–1 string Continuum potential Statistical equilibrium	Interaction particle–N strings Continuum potential Statistical equilibrium	Interaction particle–N strings Continuum potential	Interaction particle–1 atom	Interaction particle–N atoms
Information					
Flux	$n(\vec{r})$	$n(\vec{r})$	$n(\vec{r},z)$	$n(\vec{r},z)$	$n(\vec{r},z)$
Close-encounter yield	$\chi(\psi_e)$	$\chi(\psi_e)$	$\chi(\psi_e,z)$	$\chi(\psi_e,z)$	$\chi(\psi_e,z)$
References	1,15	6,7	1,8,9,10,11,12 This work	1,2,4,17,25,27	1

potential $U(r)$, the so-called string potential. In this case a classical description is applicable if[15]

$$\tfrac{1}{2}\pi\,(M_1/m)^{1/2}(Z_1 Z_2^{1/3} a_0/d)^{1/2} > 1\,.$$

This condition is fulfilled for all particles of mass large compared to the electron mass.

B. Particle-crystal interaction: The multistring hypothesis

If $U(x,y,z)$ is the potential experienced by a particle $(M_1, Z_1 e)$ moving in an atomic lattice the classical equations of motion in a Cartesian frame xyz, where z is parallel to a channel axis, can be written

$$M_1 \frac{d^2x}{dt^2} = -\frac{\partial U}{\partial x} = q\mathcal{E}_x\,,$$

$$M_1 \frac{d^2y}{dt^2} = -\frac{\partial U}{\partial y} = q\mathcal{E}_y\,,$$

$$M_1 \frac{d^2z}{dt^2} = -\frac{\partial U}{\partial z} = q\mathcal{E}_z\,,$$

where $x(t)$, $y(t)$, $z(t)$ are the coordinates of the particle, $\vec{\mathcal{E}}$ $(\mathcal{E}_x, \mathcal{E}_y, \mathcal{E}_z)$ is the electric field and its components, and $q = Z_1 e$ is the electric charge of the incoming particle.

If the continuum approximation is used the potential has no dependence on z and can be written $U(x,y)$. Moreover, $\partial U/\partial z = 0$ and the motion along the z direction is given by $z = v_z t + z_0$. Then the trajectory can be described by solving the equations of the projected motion on the xy plane.

The potential $U(x,y)$ is calculated from the multistring method. Defining a string potential $U(\vec{r} - \vec{r}_i)$ for an isolated atomic row located at position $\vec{r}_i$ in the transverse plane (Fig. 1), the total potential is the sum of the different potentials created

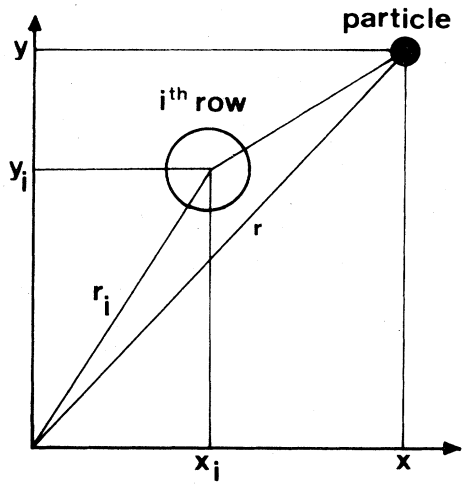

FIG. 1. Definition of geometric terms used in the formulas.

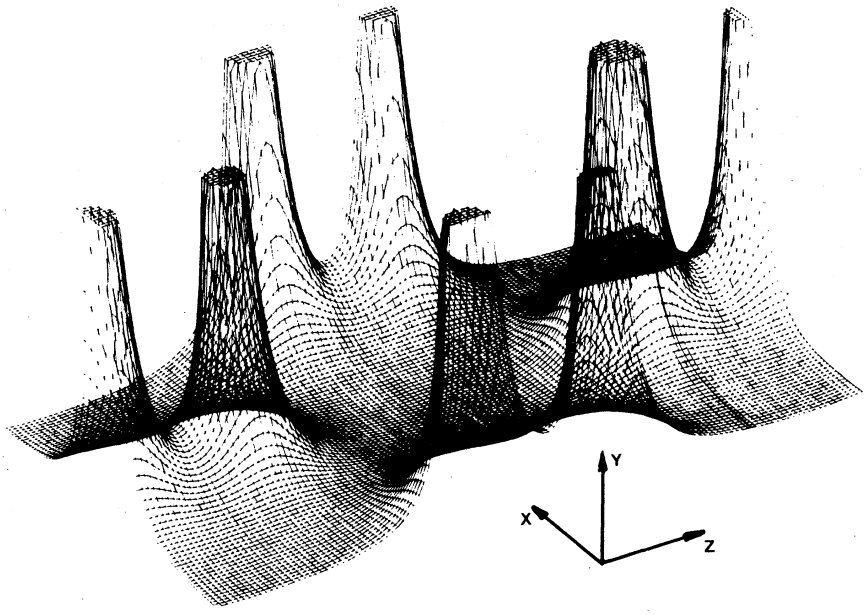

FIG. 2. Multistring calculation of potential energy for 2-MeV α particles in the $\{110\}$ transverse plane of zinc telluride. The horizontal x-z plane of the figure is the transverse plane. The magnitude of the potential is reported on the vertical direction.

by each string:

$$U(x,y)=\sum_{i=1}^{n} U(\vec{r}-\vec{r}_i)\,.$$

The number of strings has been fixed at $n=36$. It was determined that the variation of the potential was negligible when adding higher-order strings. In all cases, the Lindhard string potential[15] was used,

$$U(\vec{r}-\vec{r}_i)=\frac{Z_1Z_2e^2}{d}\ln\left(\frac{C^2a^2}{|\vec{r}-\vec{r}_i|^2}+1\right).$$

An example of a multistring potential is given for a $\langle 110\rangle$ axis of a zinc-telluride crystal (zinc-blende structure) in Fig. 2.

It is also possible to determine at any point of the transverse plane the electric field produced by the whole set of strings. From the Lindhard potential, the electric field for an isolated row is

$$\vec{\mathcal{E}}(\vec{r}-\vec{r}_i)=-\frac{Z_2e}{d}\frac{2C^2a^2}{(\vec{r}-\vec{r}_i)(|\vec{r}-\vec{r}_i|^2+C^2a^2)}\,.$$

The total field $\vec{\mathcal{E}}$ is deduced and its x component is

$$\mathcal{E}_x=-\frac{Z_2e}{d}\sum_{i=1}^{n}\frac{2C^2a^2(x-x_i)}{[(x-x_i)^2+(y-y_i)^2+C^2a^2][(x-x_i)^2+(y-y_i)^2]}\,.$$

A similar expression is obtained for the y component $\mathcal{E}_y$.

The values of $\mathcal{E}_x$ and $\mathcal{E}_y$ are thus reported in the equations of motion.

C. Method of calculation

The equations of the particle motion are solved numerically with the following initial conditions concerning the position $\vec{r}(x,y,z)$ and the velocity $\vec{v}(v_x,v_y,v_z)$ of the incident particles.

At $t=0$, $x=x_0$, $y=y_0$, $z_0=0$, and $v_{x0}=v_0\sin\theta_0\cos\varphi_0$, $v_{y0}=v_0\sin\theta_0\sin\varphi_0$, $v_{z0}=v_0\cos\theta_0$. θ_0 and φ_0 are the initial values of the θ and φ angles defined in Fig. 3 and $v_0=(2E_0/M_1)^{1/2}$, where E_0 is the energy of the incident beam. Comparing with experimental procedures we note that the angle φ is generally fixed and defines the scanning plane. The tilting angle θ is then varied for fixed φ.

The program computes the next values of the $\vec{r}$ and $\vec{v}$ components after a time interval Δt. More generally between the moments t and $t+\Delta t$, the relation between the components of $\vec{r}(t)$ and $\vec{r}$

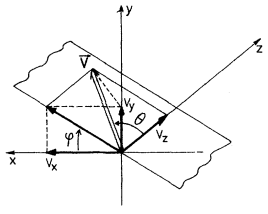

FIG. 3. Definition of angles between the direction of the particle motion and the coordinate axes.

$(t+\Delta t)$ is

$$x(t+\Delta t)=x(t)+v_x(t)\Delta t+(q\mathcal{E}_x/2M_1)(\Delta t)^2,$$

$$y(t+\Delta t)=y(t)+v_y(t)\Delta t+(q\mathcal{E}_y/2M_1)(\Delta t)^2,$$

$$z(t+\Delta t)=z(t)+v_z(t)\Delta t\,.$$

The velocities are given by

$$v_x(t+\Delta t)=v_x(t)+(q\mathcal{E}_x/M_1)\Delta t\,,$$

$$v_y(t+\Delta t)=v_y(t)+(q\mathcal{E}_y/M_1)\Delta t\,.$$

$$v_z(t+\Delta t)=(v_z^2(t)-2\Delta E/M_1)^{1/2},$$

where $\Delta E=(dE/dz)_c[z(t+\Delta t)-z(t)]$, and $(dE/dz)_c$ is the energy loss of the channeled particles. The calculation is performed for 1300 particles uniformly distributed over the transverse plane x, y. The area of the useful transverse zone is equal to that of a unit cell (or one half of a unit cell in the case of diatomic crystals).

The accuracy of the procedure depends on the time integration step Δt. In practice, Δt was chosen as large as possible to save computation time with the condition that the energy of particles was conserved. This energy conservation has been checked for many cases and it has been found that the choice of Δt depends strongly on the particle position. Defining the transverse energy by

$$E_\perp=\tfrac{1}{2}M_1(v_x^2+v_y^2)+U(x,y)\,,$$

and the relative error by

$$\Delta E_\perp/E_{\perp 0}=(E_\perp-E_{\perp 0})/E_{\perp 0}\,,$$

where $E_{\perp 0}$ is the initial transverse energy, we have computed $\Delta E_\perp/E_{\perp 0}$ for different initial impact parameters y_0. For example, the case of α particles entering the $\langle 110\rangle$ axis of a ZnTe crystal has been treated. The $\Delta E_\perp/E_{\perp 0}$ quantity has been reported (Fig. 4) as a function of the parameter $R=1-y_0/y_i$. In this latter formula, y_i is the position of the tellurium row located on the y axis (see inset, Fig. 4) and y_0 is the initial position of a particle on the same axis. It is remarked that the smaller R (concerning a particle entering the crystal near the row), the greater $\Delta E_\perp/E_{\perp 0}$. To insure a good energy conservation it is necessary to choose a time step as small as 10^{-16} sec. Such an order of magnitude for Δt has been used in computations.

D. Energy loss

The energy loss depends on the impact parameter because the electron density in the channel

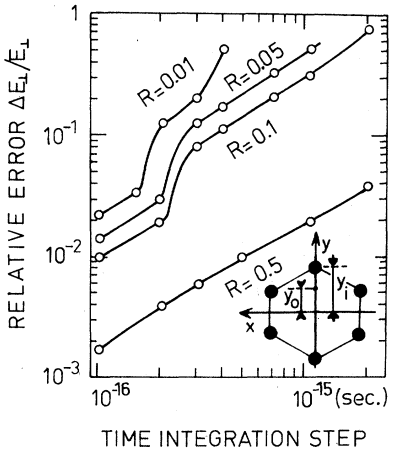

FIG. 4. Accuracy of the computational procedure as a function of time integration step for various impact parameters. The R quantity is defined in Sec. IIC.

is varying. Two relations are available to calculate the energy loss of channeled particles. The first, from Lindhard,[15] has a simple expression but overestimates the energy loss. In the second, from Appleton *et al.*[16] many parameters must be determined with specific experiments. The formalism of Lindhard has been adopted but the expression of the energy loss has been modified to introduce modifications suggested by Appleton *et al.* This procedure leads to the formula

$$\left(\frac{dE}{dz}\right)_c=\frac{2\pi Z_1^2e^4}{M_1v^2}\left(NZ_v\ln\frac{2mv^2}{\hbar\,\omega_p}+\langle NZ_c(x,y)\rangle_{\rm av}\ln\frac{2mv^2}{I}\right),$$

where ω_p is the plasma frequency, Z_v is the number of valence electrons per atom, and $\langle NZ_c(x,y)\rangle_{\rm av}$ is the mean electron density near the atomic rows. This quantity is calculated from the density of an isolated row, $\rho(r)$, through the Poisson equation using the Lindhard potential. In summing the contribution of n rows we obtain the expression

$$\langle NZ_c(x,y)\rangle_{\rm av}=\frac{Nd}{n}\sum_{i=1}^{n}\rho[(x-x_i)^2+(y-y_i)^2]\,.$$

It is of interest to introduce into this formula the random stopping power $(dE/dz)_R$. When the value of $(dE/dz)_R$ corresponds to the Bethe region the channeling stopping power can be written

$$\left(\frac{dE}{dz}\right)_c=\tfrac{1}{2}\left(\frac{dE}{dz}\right)_R\left(\frac{Z_v}{Z_c}+\frac{C^2a^2}{n\pi}\times\sum_{i=1}^{n}[(x-x_i)^2+(y-y_i)^2+C^2a^2]^{-2}\right).$$

The advantage of this formula is to allow the use of the $(dE/dz)_R$ experimental values.

E. Information displayed by the program

After each step of the program the particle coordinates x-y in the transverse plane are available. From these quantities are deduced:

(i) the particle trajectory in the whole space and in the transverse plane;

(ii) the number of particles in a surface element ΔS of the transverse plane which leads to the particle density in the channel $n(x, y, z)$.

(iii) the close-encounter probability $P(x, y)$ calculated from the distribution of atoms inside a channel. The expression introduced by Barrett[17] was used:

$$P(x, y) = \frac{\cos\psi}{2\pi u_1^2} \sum_{i=1}^{n} \exp\left(- \frac{(x - x_i)^2 + (y - y_i)^2}{2u_1^2} \right),$$

where u_1^2 is the mean-square one-dimensional vibrational amplitude;

(iv) the close-interaction yield $\chi(z)$ deduced from the close-encounter probability through the formula

$$\chi(z) = K \int\int_S P(x, y, z)\, dx\, dy,$$

where K is a normalization constant and S the channel area;

(v) the total yield χ within a depth l:

$$\chi = \int_0^l \chi(z)\, dz; \text{ and}$$

(vi) the yield of close-interaction processes from impurity atoms.

If x_I, y_I are the coordinates of the mean position of the impurity in the transverse plane, the value of the yield at a depth z is given by

$$\chi_I(z) = K_I \int\int_S P_I(x, y, z,)\sigma(x, y, z) \times n(x, y, z)\, dx\, dy.$$

$P_I(x, y, z)$ is the spatial probability distribution of the impurity.

If $C(z)$ is the macroscopic concentration profile and assuming a Gaussian distribution in the transverse plane centered at the x_I, y_I position, $P_I(x, y, z)$ can be obtained,

$$P_I(x, y, z) = C(z) f(x - x_I, y - y_I),$$

with

$$f(x - x_I, y - y_I) = \frac{1}{2\pi u_I^2} \exp\left(- \frac{(x - x_I)^2 + (y - y_I)^2}{2u_I^2} \right),$$

where u_I^2 is the mean-square one-dimensional vibrational amplitude of the impurity atoms.

The quantity $\sigma(x, y, z)$ is the nuclear cross section and following Carstanjen and Sizmann is given by[18]

$$\sigma(x, y, z) = \sigma(z)\delta(x - x_I)\delta(y - y_I),$$

where $\sigma(z)$ is determined by the values of $\sigma(E)$ (excitation curve) and $(dE/dz)_c$ (energy loss).

(vii) The total interaction yield curve obtained within a fixed depth is

$$\chi_I = \int_0^l \chi_I(z)\, dz.$$

From specifications (v) and (vii) the angular distributions relative to the substrate and to the impurity are calculated by varying the incident angles φ and/or θ.

III. PROBLEM OF THERMAL VIBRATIONS

The displacement of atoms from their equilibrium sites by thermal vibrations influences the trajectories through a modification of the net potential and of the close-encounter probability.

A. Influence of thermal vibrations on trajectories

Following the method adopted by Andersen and Feldman[19] with a Thomas-Fermi-Molière potential it has been assumed that the thermal vibrations lead to an averaging of the one-string potential obtained by convolution of the Lindhard potential with the displacement probability distribution of the atoms $f(\rho')$

$$V(r) = \frac{Z_1 Z_2 e^2}{d} \int_0^{+\infty} d\rho' \int_0^{2\pi} f(\rho') U(\rho'^2 + r^2 - 2\rho' r \cos\theta)\, d\theta,$$

where ρ' is the distance between the dynamic position and the rest position of the atom. If one approximates $f(\rho')$ by a Gaussian probability with a variance u_2^2, one obtains

$$f(\rho') = (2\rho'/u_2^2) \exp(-\rho'^2/u_2^2).$$

The integration is performed numerically except for $r = 0$. In this case $V(0)$ can be obtained analytically:

$$V(0) = (Z_1 Z_2 e^2/d) \ln[w + \mathrm{Ei}(w)\, e^w + \gamma].$$

$w = 3a^2/u_2^2$, γ is the Euler constant, and Ei the exponential integral. Results for a ZnTe crystal are shown in Fig. 5. However, the significance of this approach is questionable. Indeed, in comparing

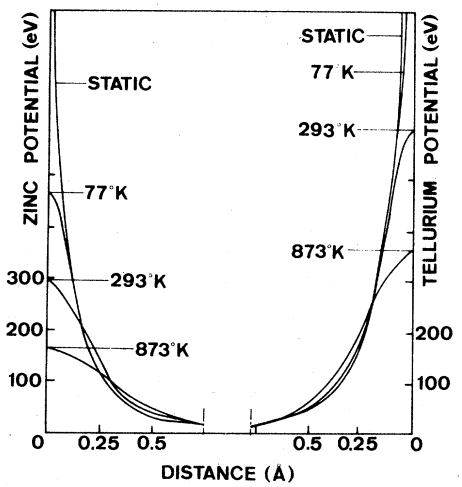

FIG. 5. String potential of zinc and tellurium rows in a ZnTe crystal, taking account the thermal vibrations of the lattice atoms.

the minimal period of thermal vibrations to the transit time of particles, it is clear that the particles are moving in a static lattice of which the atomic rows have light curvature corresponding to the phonon propagation. The potential depends on the penetration depth and the equations of motion are modified from one given depth to the following. There is no simple way to take into account such a potential modification by thermal vibrations for which the convolution method is not realistic. Thus, in a first approximation this phenomenon will be neglected in our calculation.

B. Influence of thermal vibrations on the close-encounter probability

The definition given in Sec. II E holds. Indeed, the close interactions occur in different channels at different times and there is no correlation between the atomic displacements and the depth where the close process is occurring.[20] The atomic displacement probability can be chosen as a Gaussian with a variance u_2^2 centered on the mean position of atoms.

C. Determination of the mean-square deviation

1. Monatomic crystals

The mean-square deviation of the atomic displacement probability can be deduced from the measurements of the Debye temperature Θ_D, as it is usual in channeling computer simulation.[1] The Θ_D values given by the neutron or x-ray diffraction experiments are preferred to those given by the specific-heat measurements because the frequency spectrum is weighted in different ways.[21] The mean-square vibrational amplitude perpendicular to an axis is given by

$$u_2^2 = \tfrac{2}{3}\langle u^2\rangle ,$$

with

$$\langle u^2\rangle = \frac{9\hbar^2}{kM_2\Theta_D}\left(\frac{\phi(X_m)}{X_m}+\frac{1}{4}\right),$$

where $X_m = \Theta_D/T$, T is the absolute temperature, and $\phi(X_m)$ is the Debye function

$$\phi(X_m) = \int_0^{x_m} \frac{x\,dx}{e^x - 1}.$$

2. Diatomic crystals

It is said by Hosemann and Bagchi[22] that the formula defined in Sec. II holds when a lattice cell consists of different atoms possessing different displacement statistics. In this case they write the mean-vibrational amplitude

$$\langle u_i^2\rangle = \frac{9\hbar^2}{kM_i\Theta_i}\left(\frac{\phi(X_i)}{X_i}+\frac{1}{4}\right),$$

where the subscript $i = A,B$ indicates the type of atom. It appears that we need two characteristic temperatures Θ_A and Θ_B, but only one is available from experimental data. These authors give an example where they assume a common value $\Theta_i = \Theta_D$ for the two atomic species and where only M_i is varying in determining $\langle u_i^2\rangle$. This is the procedure followed by Morgan and Jackson,[5] and in the same way we give the example of ZnTe in Fig. 6.

Another way to introduce the vibrational amplitudes is to use values published in the literature, either experimental or theoretical from lattice dynamical models. This procedure has many disadvantages: the lack of experimental data and the differences between results of theoretical models for the same crystal. This is illustrated in Fig. 6. In order to avoid these problems and to be able to compare the computer simulations with one another we have calculated the thermal vibrations using a simplified model.

3. One-dimensional model

The model is the simplest one: the one-dimensional lattice of which a detailed study is found in the treatise of Brillouin and Parodi.[23] Let

$$u_{2n+1} = X_A \exp[\,i\omega t - (2n+1)\,qd\,],$$

$$u_{2n} = X_B \exp(i\omega t - 2nqd),$$

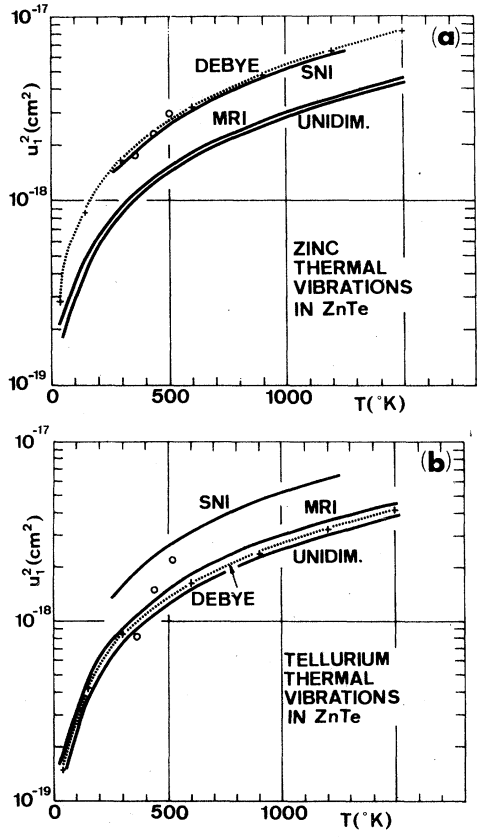

FIG. 6. (a) Zinc thermal vibration amplitude in a ZnTe crystal as a function of temperature. UNIDIM: one-dimensional model; DEBYE: Debye model, MRI: modified rigid-ion model; SNI: second-neighbor-ion model. Experimental points (o) are also indicated. (b) Tellurium thermal vibration amplitude in a ZnTe crystal as a function of temperature. Definitions of symbols as in (a).

be the displacements of A and B type atoms. In these formulas q is the wave number and d the distance between two closest identical atoms. The cited authors determine the amplitude ratio

$$R=\frac{X_A}{X_B}=\frac{M_A-M_B\pm[(M_A+M_B)^2-4M_AM_B\sin^2qd]^{1/2}}{2M_A\cos qd}.$$

The amplitudes X_A and X_B can be found from the energy conservation law

$$\tfrac{1}{2}(M_AX_A^2+M_BX_B^2)\omega^2=\hbar\omega,$$

yielding

$$X_A^2=\frac{2\hbar}{\omega}\frac{1}{M_A+M_B/R^2},$$

$$X_B^2=\frac{2\hbar}{\omega}\frac{1}{M_A+M_BR^2}.$$

To determine the mean-square displacement we assume that the displacement is given by the one-dimensional model but we calculate the number of vibration modes for a three-dimensional solid,

$$\langle u_i^2\rangle=3N\int_0^{q_M}X_i^2n(q)\frac{q^2dq}{2\pi},\quad i=A,B,$$

N is the atomic density, q_M is the maximal value of q, and $n(q)$ the Bose distribution;

$$n(q)=\tfrac{1}{2}+[\exp(\hbar\omega/kT)-1]^{-1}.$$

The integration is performed numerically. Results concerning ZnTe are shown in Fig. 6 together with experimental data and results from lattice-dynamical models. The values obtained for the one-dimensional model are in good agreement with those obtained from the others (model of rigid ions, MRI[24]; second-neighbor-ion model, SNI[25]).

IV. RESULTS AND DISCUSSION

Due to its nature, the multistring model can be applied at a given axis of a given crystalline structure. Computations were performed for the following axes shown in Fig. 7: (i) monatomic crystals: ⟨110⟩ axis of fcc and diamond structure, ⟨100⟩ axis of fcc and bcc structure, C axis of hexagonal structure; (ii) diatomic crystals: ⟨110⟩ axis of zinc-blende structure. These axes are easily treated by the same program because the ⟨110⟩ diamond structure axis is constituted of two ⟨110⟩ zinc-blende structure axis.

A. Trajectories

A preliminary computation was carried out for 1.5-MeV α particles entering the ⟨110⟩ axis of a GaP crystal (zinc-blende structure). The particles initially located on the {110} plane parallel to this axis (the projection of this plane on the transverse plane is the a-b line seen in Fig. 7) were considered for comparison with other computations. The results reported in Fig. 8 exhibit the oscillating character of trajectories, and we can deduce a wave-length λ depending on the initial distance to an atomic row. This dependence with the initial impact parameter has been traced for particles initially located on the {110} plane already defined. It is seen in Fig. 9 that the general form of the curve is in qualitative agreement with the one calculated by Abel *et al.*[19] in a planar case. It is noteworthy that the wavelength of trajectories initiated near the channel center tends to a limiting value λ_M which does not correspond to the harmonic limit given by the Van Vliet formula,[26]

$$\tfrac{1}{4}\lambda_v=\pi r_0^2/\psi_1Ca\sqrt{n},$$

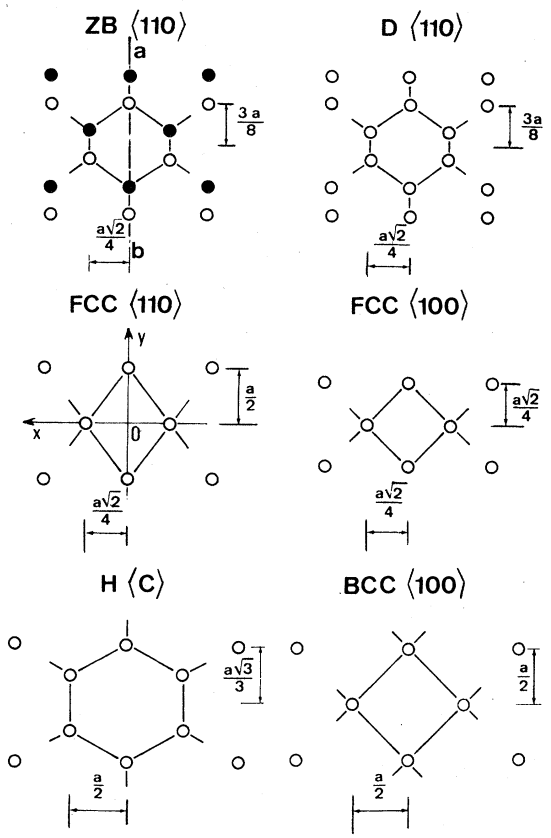

FIG. 7. Channel geometries used in the multistring program. The origin of the x-y frame is located at the center of each channel as shown for the ⟨110⟩ channel of fcc structure. The a-b line across the ⟨110⟩ channel of the zinc-blende structure defines the {110}-type plane considered in the text.

where n is the number of atomic rows surrounding a channel of radius r_0. In all crystals we have considered we find the approximate relation $\lambda_v \simeq 0.65\ \lambda_M$. This result can be explained by noting that for the diamond or zinc-blende structure the multistring potential at the channel center is not symmetric.

B. Particle flux inside a channel

From the particle trajectories we are able to determine the spatial density of particles $n(x, y)$ in the transverse plane at each stop of the program i.e., a given depth z beneath the crystal surface. The quantity $n(x, y)$ was calculated by dividing the channel cross section S in elemental square areas ΔS and recording the number of ions passing through each elemental area. For the following calculations a ratio $\Delta S/S = 7 \times 10^{-3}$ was used.

We have investigated numerous axes and the flux variation with depth is illustrated in Fig. 10, where the flux at the channel center is measured in the

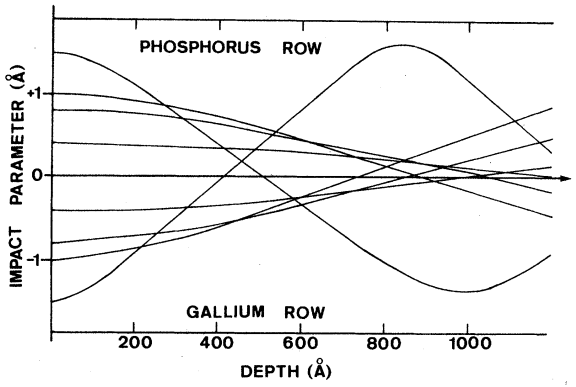

FIG. 8. Trajectories of 1.5-MeV α particles entering the ⟨110⟩ axis of GaP with $\theta_0 = \varphi_0 = 0°$. The initial parameters are situated on the {110}-type plane shown in Fig. 7.

case of zinc-blende structure crystals (GaP and ZnTe). A pronounced flux peaking effect appears for the following mean depth $\bar{z}$:

$\bar{z}$(GaP) $\simeq$ 1020 Å (α particles, 1.5 MeV),

$\bar{z}$ (ZnTe) $\simeq$ 1280 Å (α particles, 2 MeV).

This depth corresponds to a mean wavelength

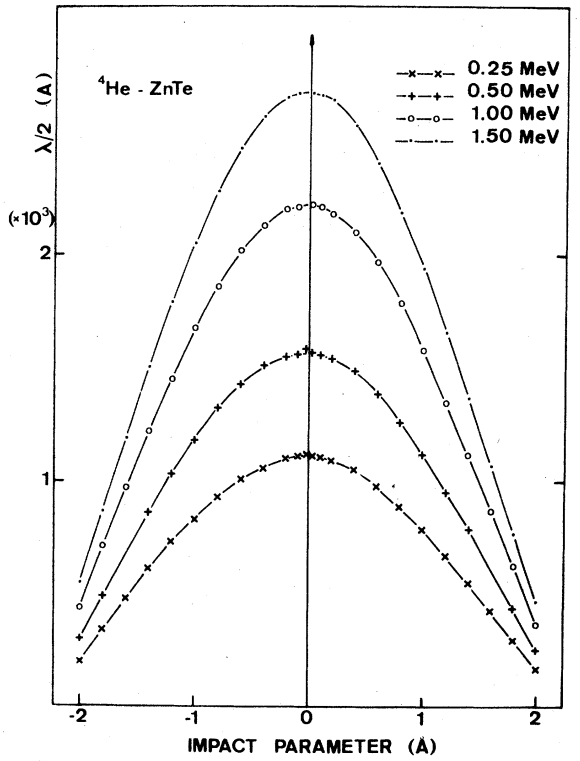

FIG. 9. Half wavelength of the particle trajectories in the {110}-type plane defined in Fig. 7, as a function of the initial-impact parameter (initial conditions: $\theta_0 = \varphi_0 = 0°$).

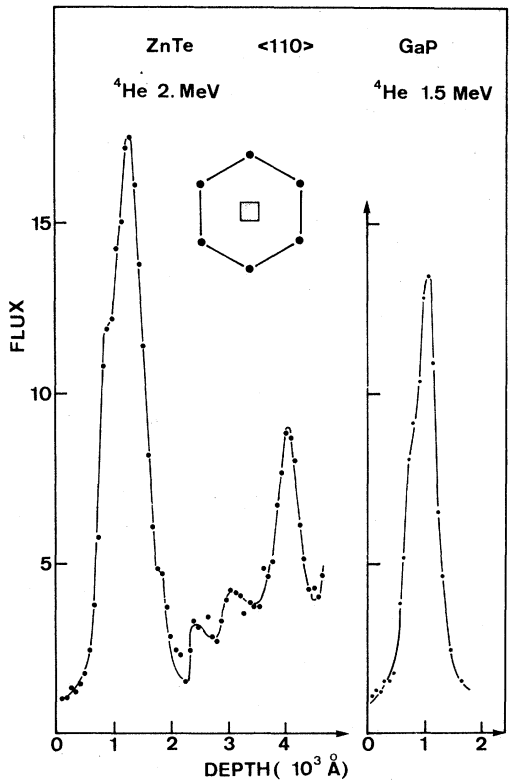

FIG. 10. Variation of the α-particle flux as a function of penetration depth in $\langle 110 \rangle$ channels of ZnTe and GaP (initial conditions: $\theta_0 = \varphi_0 = 0°$).

$\bar{\lambda}/4$, which can be compared to the values obtained in the preceding section. We find that $\bar{\lambda} < \lambda_M$ ($\bar{\lambda} = 0.86\lambda_M$ for GaP and $\bar{\lambda} = 0.94\ \lambda_M$ for ZnTe). This is explained in defining the mean wavelength with the formula

$$\bar{\lambda} = \frac{1}{\pi r_0^2} \int_0^{r_0} \lambda(r_i)\, 2\pi r_i\, dr_i \ ,$$

where r_i is the initial distance to the channel center. If we assume cylindrical symmetry and a parabolic variation of $\lambda(r_i)$ with r_i, the $\bar{\lambda}$ value is of the order of $\frac{1}{2}(\lambda_M + \lambda_{\min})$.

Moreover, as a test of the validity of the method we have computed the flux for 1.5-MeV α particles in the $\langle 110 \rangle$ channel of copper. We have compared our results with the results obtained by Alexander and Poate using a binary collision model in the same conditions.[27] Figure 11 shows the values of the two fluxes at the center of the channel. The gross features of the two fluxes are in relative agreement, i.e., the maxima occur for neighboring depths. However, two principal points can be made: (i) The maximum of the multistring program occurs at a greater depth than for the binary collision model; and (ii) After the first peak, the

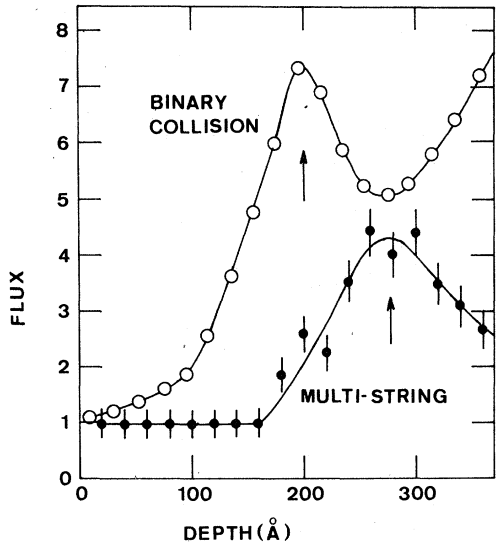

FIG. 11. Variation of the α-particle flux in the $\langle 110 \rangle$ channel of copper as a function of penetration depth. Comparison between the multistring and the binary collision model results.

flux of the multistring program shows a very rapid falloff, whereas the flux computed from the binary collision model stays at a rather high level.

The first effect seems due to the choice of the potential. Indeed, the Lindhard potential is more flat bottomed than the Molière potential used in the calculations of Alexander and Poate. If we approximate the two potentials with a harmonic one we find that the Lindhard potential leads to a lower value of the k constant, and thus to a greater value of λ. The second difference is not clearly understood but could be due to neglecting multiple scattering in the multistring model.

In the study of the impurity location in a lattice, the incident angle is varying. Figure 12 shows the

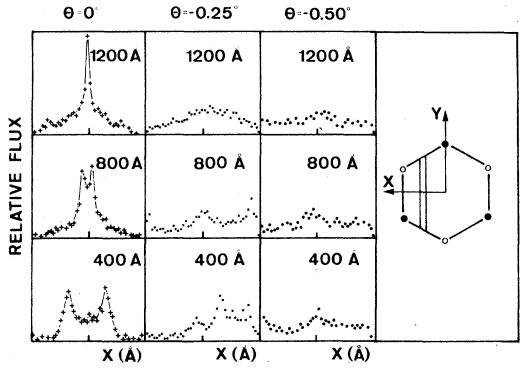

FIG. 12. Variation of the 2-MeV α-particle flux (computed over the dashed area) in a $\langle 110 \rangle$ channel of a ZnTe crystal, as a function of the incident angle and the penetration depth.

effects of such a variation on the flux distribution over the transverse dimension x of the channel. The dependence of the impurity close-interaction yield with depth, the incident angle and the impurity position is clearly seen.

C. Close-encounter yield

The close-encounter yield $\chi(z) = \iint P_0(x, y) \times n(x, y, z)\, dx\, dy$ has been computed for different incident angles (φ_0, θ_0). The integration is performed with the two-dimensional grid already used for the flux. The program allows one to treat monatomic as well as diatomic rows. In this latter case, a diatomic row made up of A and B atoms is considered as a string with an average charge $\frac{1}{2}(Z_A + Z_B)$. For channels bordered by different monatomic rows the program computes separately the contribution of the A or B rows and displays the two yields $\chi_A(z)$ and $\chi_B(z)$. The results presented here concern essentially the ⟨110⟩ channel of diamond and zinc-blende structure crystals. The silicon case has been considered, and the depth-dependent interaction yield is represented in Fig. 13. Large variations of the yield are seen which can be related to backscattering spectra. In contrast, the weak amplitude oscillations are not representative of a physical effect but are due to the simplicity of the model which does not take into account the smearing of the flux due to the multiple scattering. Also in Fig. 13, the angular dependence of the yield is shown. From such curves we can deduce the angular distribution $\chi(\theta)$.

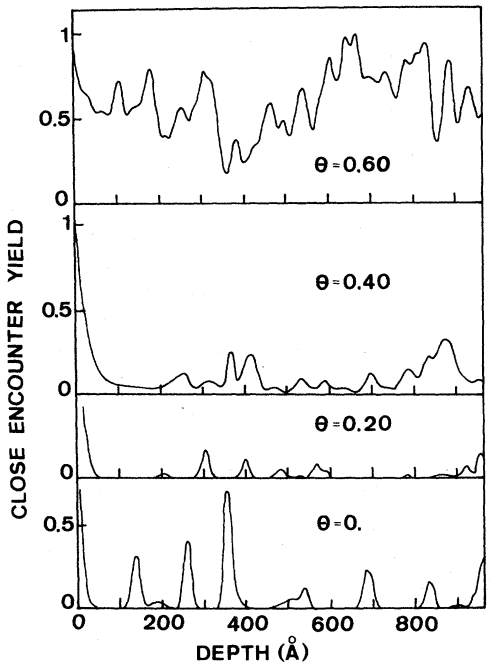

FIG. 13. Close interaction yield calculated as a function of depth for 2-MeV α particles entering a ⟨110⟩ channel of a silicon crystal.

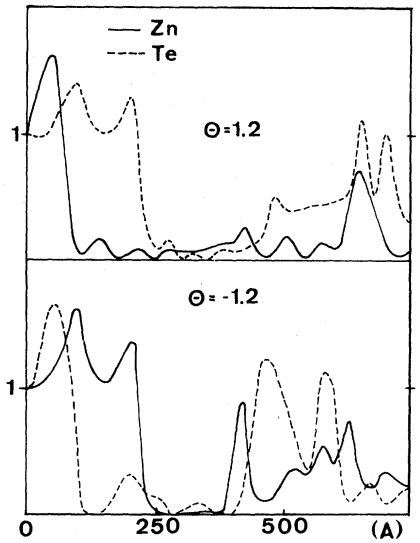

FIG. 14. Close interaction yield calculated as a function of depth for 1.3-MeV protons entering a ⟨110⟩ channel of a ZnTe crystal.

For diatomic compounds characteristic curves have been extracted from our results. In Fig. 14 we show the close-encounter yields relative to zinc and to tellurium for 1.3-MeV protons entering the ⟨110⟩ axis of ZnTe with the initial conditions $\varphi = 90°$ and $\theta = \pm 1.2°$. It is apparent that, for $\theta = 1.2°$ and near the surface, the close-encounter yield relative to tellurium is greater than that relative to zinc, whereas for $\theta = -1.2$ the yield relative to zinc is greater than the yield relative to tellurium. This balancing behavior can be explained if we consider the $\{110\}$ plane which corresponds to the scanning angle $\varphi = 90°$ (Fig. 17). Indeed, we can see that particles incoming with an angle $+\theta$ of incidence relative to the ⟨110 axis have a greater probability to strike an A row than a B row and conversely for particles with $-\theta$ incident direction. This result, which is called the phenomenon of the preferential interaction, has been verified by experiment.[28] It must be observed that this phenomenon occurs for particular tilting angles and thus, the close-encounter yield relative to the A or B atomic species is depending on the choice of the scanning direction.

D. Angular distributions

The variation with θ (for fixed φ) of the intergrated yield $\chi = \int_0^t \chi(z)\, dz$ is called the angular distribution. The only results presented here con-

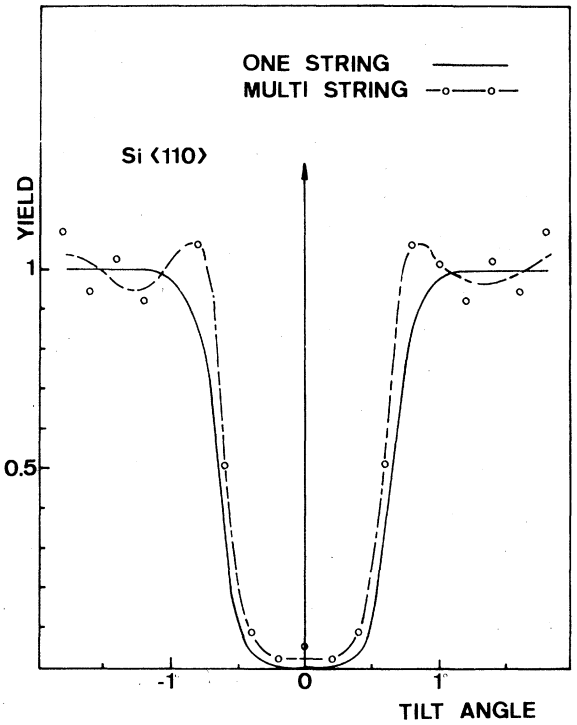

FIG. 15. Calculated angular distributions of integrated yield for 2-MeV α particles in silicon. ——— from the one-string formula; --o-- from the multistring model.

cern the ⟨110⟩ direction of the diamond (monatomic) or zinc-blende (diatomic) structure.

1. Monoatomic crystals

The variation of χ is shown in Fig. 15 for 2-MeV α particles in silicon. The scanning plane is defined by $\varphi = 40°$, and the integration depth is $l = 1300$ Å. We have also shown for comparison the curve calculated from the one-string Lindhard theory through the formula

$$\chi = \exp \frac{-(C^2 a^2/u_2^2)}{[\exp(2\theta^2/\psi_1^2) - 1]}.$$

TABLE II. Comparison of theoretical and experimental values of half-width angles $\theta_{1/2}$.

Crystal	$\theta_{1/2}$ values for 2-MeV α particles in ⟨110⟩ axis		
Silicon	Lindhard	Multistring	Experimental (from Ref. 29)
	0.64	0.59	0.55
Zinc telluride			Experimental (from Ref. 30)
Zn		0.63	0.51
Te		0.83	0.70

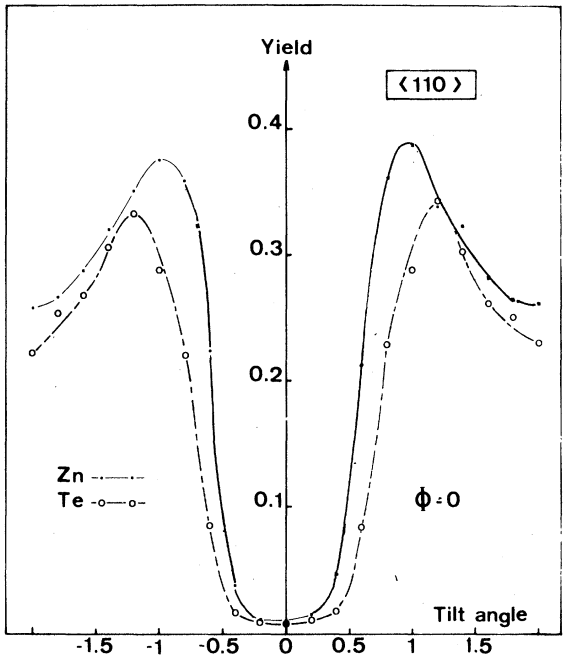

FIG. 16. Calculated angular distributions of integrated yield for 2-MeV α particle in zinc telluride. -·-·- relative to the zinc rows, -o-o- relative to the tellurium rows.

From this expression we can obtain the half-width at medium height of the distribution $\theta_{1/2}$. In the Table II are given the $\theta_{1/2}$ values deduced from the multistring program, the preceding formula, and from the experiment. The multistring program value is higher than the experimental one. This is due to neglect of the multiple scattering.

2. Diatomic crystals

For channels bordered with two different monatomic rows, two different angular distributions are obtained. Figure 16 represents the Zn and Te yields for 2-MeV α particles in ZnTe at $\varphi = 0$ and $l = 1300$ Å. The scanning angle $\varphi = 0$ has been chosen to avoid the preferential interaction. In this case, the scan occurs along the {100} plane and a strong shoulder is obtained at the axial-planar transition. As for monatomic crystals, experimental and theoretical half-widths are compared (table II). The multistring values are again greater than experimental one for the same reason. However, in all cases the following ratio holds:

$$\theta(\mathrm{Zn})/\theta(\mathrm{Te}) = (Z_2(Zn)/Z_2(Te))^{1/2} = 0.76\,.$$

The preferential interaction evidenced in the calculation of the close-encounter yield is also seen in the angular distributions. For 1.5-MeV α

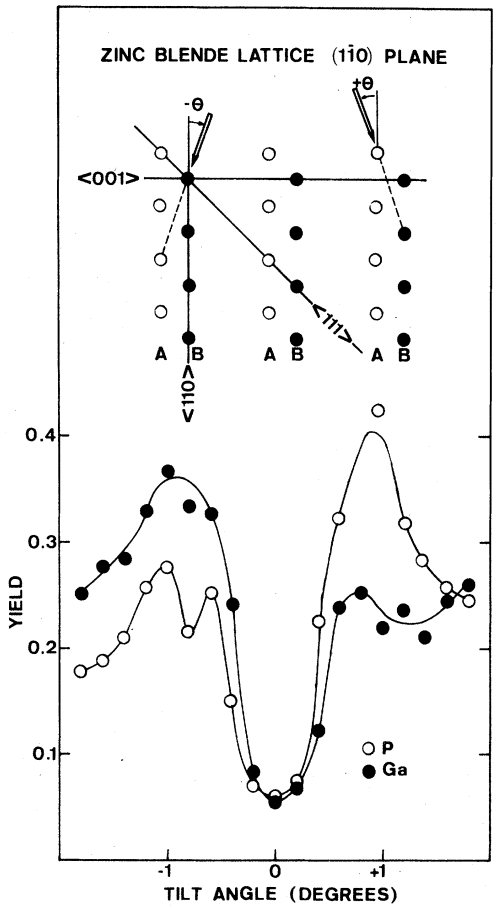

FIG. 17. Calculated angular distributions of integrated yield for 1.5-MeV α particles in gallium phosphide. The entrance angles and the tilting plane are chosen to exhibit the preferential interaction.

particles in a ⟨110⟩ axis of GaP, an asymmetric dip is obtained if a scan is performed at $\varphi = 90°$ (Fig. 17). Moreover, for an angle $\theta \simeq 1°$, the P curve exhibits an enhancement which corresponds to a slight decrease of the Ga curve and vice versa for $\theta \simeq -1°$. We can explain this behavior in noting that for $\theta \simeq 1°$, the incident particles interact in preference with the P rows and for $\theta \simeq -1°$ with the Ga rows, as already evidenced for Zn and Te rows of ZnTe.

E. Application to lattice location of impurities

It has been already shown that complete angular scans should be done in plotting the yield χ_I of close interactions specific to the impurity to locate this impurity in a lattice.[27] The program computes the yield χ_I for one or more foreign atoms inside the channel. Many cases have been considered and two typical examples are given

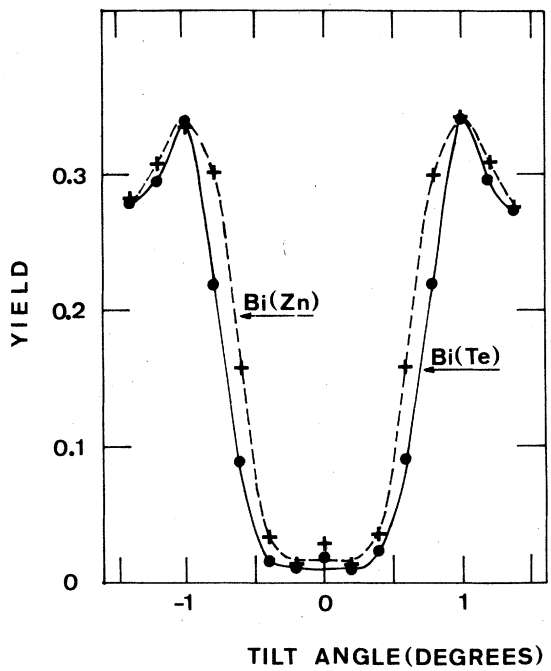

FIG. 18. Calculated angular distributions relative to a substitutional impurity in a ZnTe crystal. --+-- Bi on zinc site, —●— Bi on Tellurium site.

1. Substitutional impurity in a diatomic lattice

As shown by Mertz *et al.*, if an impurity is in substitution of a given atomic species the angular distribution relative to this atomic species and that relative to the impurity are similar.[31] To verify this conclusion and also to interpret an experiment on the lattice location of implanted Bi in zinc telluride,[32] yield curves for Bi impurities in Zn and Te sites were calculated for ⟨110⟩ axis. The mean vibrational amplitudes were chosen in defining a Debye temperature for the impurity with the formula used by Sigurd and Bjorkvist.[33]

$$\theta_I = \theta_D (M/M_I)^{1/2},$$

where M_I is the impurity atomic mass, M the averaged mass of zinc and tellurium, and θ_D the Debye temperature.

The impurity yield curves (Fig. 18) are very close to those of the substrate (Fig. 15), verifying the statement of Mertz *et al.*

2. Interstitial impurity

The ⟨100⟩ yield curves for interstitial deuterium atoms in tungsten were calculated in order to compare our results with those of Picraux.[7] Indeed, 15-KeV implanted deuterium has been found

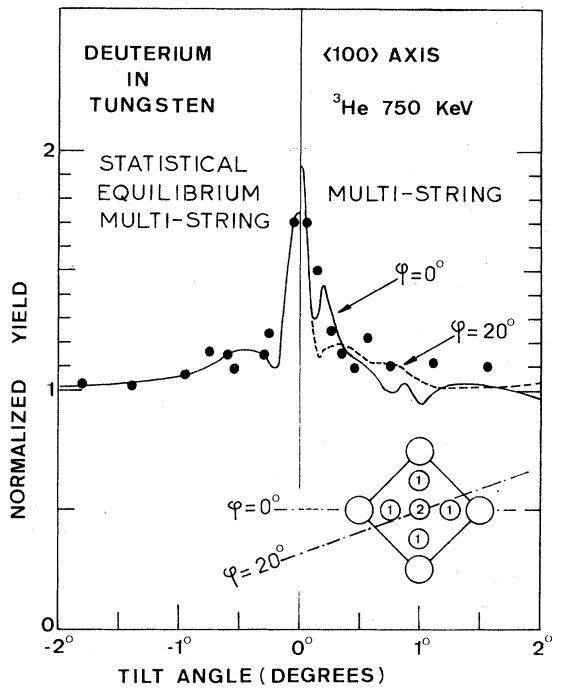

FIG. 19. Calculated angular distribution relative to interstitial deuterium in a tungsten crystal. Experimental points from Picraux (Ref. 7). Theoretical curves: left-hand side, from Ref. 7; right-hand side, from the multistring program; —— $\varphi = 0$; – – – $\varphi = 20°$.

experimentally in tetrahedral sites by Picraux and an interpretation of the experimental curve with a statistical equilibrium multistring model has also been given by this author. In our calculus, deuterium impurities have been assumed to have a Gaussian concentration profile and their tetrahedral interstitial positions in the ⟨100⟩ channel are seen on the Fig. 19. Two scanning directions ($\varphi = 0°$ and $\varphi = 20°$) are chosen to denote their influence on the yield curve. Our results are seen on Fig. 19 together with experimental points. The theoretical curve from statistical equilibrium multistring analysis[7] is also shown. It can be stated that our theoretical curves present a fairly good agreement with experimental points. The structure of our calculated curve can be analysed. The central peak is due to the contribution of the impurities located at the channel center (0 site) while the two lateral little peaks to that of the impurities located on peripheric sites. The two theoretical curves present two differences: the amplitude of the central peak and the position of the two lateral peaks. The central peak of the Picraux' s curve is lower because at the statistical equilibrium the flux is averaged over the whole depth and there is no flux peaking effect with depth which enhances the yield. The position of the two lateral peaks depends on the value of the scanning direction (φ angle). This position varies with the φ angle in our calculation, whereas it is averaged on the all φ angles in the statistical equilibrium multistring model.

V. CONCLUSIONS

A model has been presented to study the interaction of particles with atomic rows and with foreign atoms in a crystal. This model is essentially based on the two following assumptions: (i) the actual periodic potential of an atomic row is replaced by an average potential (continuum approximation); and (ii) the total potential is the sum of many continuum potentials (multistring model). Calculations were performed in solving the classical equation of particle motion in a channel. The oscillatory character of computed trajectories leads to the concept of mean wavelength $\bar{\lambda}$. This wavelength is also evident in the calculation of the flux distribution of particles in the channel. Comparison of this flux distribution with other computer simulations shows that as a function of depth two differences arise: the first flux peak occurs at greater depth due to the use of the Lindhard potential, and after this peak the flux falls to a smaller value due to neglect of the multiple scattering effect. The close encounter yield as a function of depth has been calculated and, in the case of zinc-blende structure lattices, the preferential interaction of particles with one row type rather than the other has been evidenced. This effect is also shown in the angular distribution of the integrated yield. The model is used to locate foreign atoms in the lattice. For impurities on substitutional sites in a diatomic crystal, the conclusion of Mertz *et al.* has been verified, and for impurities on interstitial sites the results are in agreement with calculations from other models.

In summary, the main advantage of the model is its relative simplicity compared to its possibilities. Indeed, it is the simplest one which allows one to obtain the flux and the close-encounter yield as functions of the penetration depth of particles. The limitations of the model are in neglecting the effects of the multiple scattering and of the thermal vibrations on trajectories. However, taking account of the multiple scattering and the modification of the potential by thermal vibrations diminishes the analytic character of the formulas, which leads to a greatly increased volume of numerical calculations.

ACKNOWLEDGMENTS

The authors wish to thank M. Pfister and M. Ligeon for helpful comments in the preparation of this article.

[1]See, for a review: D. S. Gemmel, Rev. Mod. Phys. 46, 129 (1974); in *Channeling: Theory, Observation and Applications*, edited by D. V. Morgan (Wiley, New York, 1973).
[2]C. Varelas and R. Sizmann, Radiat. Eff. 16, 211 (1972).
[3]R. D. Edge, C. Varelas and R. Sizmann, Radiat. Eff. 16, 95 (1972).
[4]S. Roth and R. Sizmann, Radiat. Eff. 20, 43 (1973).
[5]D. V. Morgan and D. P. Jackson, Radiat. Eff. 29, 99 (1976).
[6]K. Komaki, in *Ion Beam Surface Analysis*, edited by O. Mayer, G. Linker, and F. Käppeler (Plenum, New York, 1976), p. 517.
[7]S. T. Picraux, in *Ion Beam Surface Analysis*, edited by O. Meyer, G. Linker, and F. Käppeler (Plenum, New York, 1976), p. 527.
[8]A. Bontemps, J. Fontenille, and E. Ligeon, in Proceedings of "Session sur la Canalisation," Saclay, 1974 (unpublished).
[9]Y. V. Bulgakov and V. I. Shulga, Radiat. Eff. 28, 15 (1976).
[10]Y. Hashimoto, J. H. Barrett, and W. M. Gibson, Phys. Rev. Lett. 30, 995 (1973).
[11]Y. Hashimoto, Bull. Am. Phys. Soc. 17, 560 (1972).
[12]Y. Hashimoto and J. H. Barrett, Bull. Am. Phys. Soc. 18, 119 (1973).
[13]L. T. Chadderton, Philos. Mag. 18, 1017 (1968).
[14]F. Fujimoto, S.Takagi, K. Komaki, H. Toike, and Y. Uchida, Radiat. Eff. 12, 153 (1972).
[15]J. Lindhard, K. Dan. Vidensk. Selsk. Mat.-Fys. Medd. 34, 14 (1965).
[16]J. Lindhard, K. Dan. Vidensk. Selsk. Mat.-Fys. Medd. 34, 14 (1965).
[17]J. H. Barrett, Phys. Rev. B 3, 1527 (1971).
[18]H. D. Carstanjen and R. Sizmann, Phys. Lett. A 40, 93 (1972).
[19]J. U. Andersen and L. C. Feldman, Phys. Rev. B 1, 2063 (1970).
[20]F. Abel, G. Amsel, M. Bruneaux, C. Cohen, and A. L'hoir, Phys. Rev. B 13, 993 (1976).
[21]B. W. Batterman and D. R. Chipman, Phys. Rev. 127, 690 (1962).
[22]R. Hosemann and S. N. Bagchi, in *Direct Analysis of Diffraction by Matter* (North-Holland, Amsterdam, 1969), p. 277.
[23]L. Brillouin and M. Parodi, in *Propagations des Ondes dans les Milieux Pêriodiques* (Masson-Dunod, Paris, 1956).
[24]J. F. Vetelino, S. P. Gaur, and S. S. Mitra, Phys. Rev. B 5, 2360 (1972).
[25]D. N. Talwar and B. K. Agrawal, J. Phys. C 7, 2981 (1974).
[26]D. Van Vliet, Radiat. Eff. 10, 137 (1971).
[27]R. B. Alexander and J. M. Poate, Radiat. Eff. 12, 211 (1972).
[28]A. Bontemps, J. Fontenille, and A. Guivarc'h, Phys. Lett. A 55, 373 (1976).
[29]S. T. Picraux, J. A. Davies, L. Eriksson, N. G. E. Johansson, and J. W. Mayer, Phys. Rev. 180, 873 (1969).
[30]A. Bontemps, E. Ligeon, and R. Danielou, Radiat. Eff. 22, 195 (1974).
[31]J. L. Merz, L. C. Feldman, D. W. Minguay, and W. N. Augustyniak, in *Ion Implantation in Semiconductors*, edited by I. Ruge and J. Graul (Springer-Verlag, Berlin, 1971).
[32]A. Bontemps, thesis (Grenoble, 1977) (unpublished).
[33]D. Sigurd and K. Bjorkqvist, Radiat. Eff. 17, 209 (1973).